https://doi.org/10.1021/acsami.7b00576

A Water Soluble Polymeric Interfacial Material for Planar Perovskite Solar Cells.

Lingling Zheng,[a,b] *Yingzhuang Ma,*[c] *Lixin Xiao,*[c,e,*] *Fengyan Zhang,*[a] *Yuanhao Wang*[d,*] *and Hongxing Yang*[b]

[a]School of Energy Research, Xiang'an Campus, Xiamen University, Xiamen 361100, Fujian, China.

[b]Renewable Energy Research Group (RERG), Department of Building Services Engineering, The Hong Kong Polytechnic University, Hong Kong.

[c]State Key Laboratory for Mesoscopic Physics and Department of Physics, Peking University, Beijing 100871, China.

[d]Faculty of Science and Technology, Technological and Higher Education Institute of Hong Kong, New Territories, Hong Kong.

[e]Co-Innovation Center for Micro/Nano Optoelectronic Materials and Devices, Chongqing University of Arts and Sciences, Yongchuan Chongqing 402160, P.R.China.

KEYWORDS

Interfacial materials, Water soluble, Planar perovskite solar cells, Impedance analysis, Hysteresis effect.

ABSTRACT

The interfacial materials play a critical role on the photoelectric conversion properties as well as the anomalous hysteresis phenomenon of the perovskite solar cells (PSCs). In this article, a water soluble polythiophene PTEBS was employed as a cathode interfacial material for PSCs. Efficient energy level aligning and improved film morphology were obtained due to an ultrathin coating of PTEBS. Better ohmic contact between the perovskite layer and the cathode also benefits the charge transport and extraction of the device. Moreover, less charge accumulation at the interface weakens the polarization of the perovskite resulting in a relatively quick response of the modified device. The ITO/PTEBS/$CH_3NH_3PbI_3$/spiro-MeOTAD/Au cells by an all low-temperature process achieved power conversion efficiencies of up to 15.4% without apparent hysteresis effect. Consequently, the utilization of this water soluble polythiophene is a practical approach for the fabrication of highly-efficient, large-area and low-cost PSCs, and compatible with low-temperature solution process, roll-to-roll manufacture and flexible application.

1. INTRODUCTION

Perovskite solar cells (PSCs) became one of the most attractive topic in new-generation solar cells over the past 5 years. Inorganic-organic perovskites, for example $CH_3NH_3PbI_3$ and

$CH_3NH_3PbI_{3-x}Cl_x$, exhibit very excellent optoelectronic properties, such as the intensive light absorption in the whole visible spectrum, very long carrier diffusion length and suitable band structure.[1-3] Consequently, the power conversion efficiency (PCE) of PSCs has dramatically increased to the certificated 22.1% at warp speed.[4] Much efforts have been made to control the film morphology[5-7] or develop novel materials[8,9], and significate improvements are achieved for PSCs with better performance as well as high stability.[10,11]

The interfacial material is essential as the electron transport material (ETM) or hole blocking material (HBM) between the electrode and the perovskite layer to guarantee efficient charge transport and extraction.[12,13] Otherwise, a large energy band offset of above 0.5 eV would arise if the perovskite layer is directly deposited onto the electrode, which would cause serious charge accumulation at the interface. Besides, the hysteresis effect, especially for the planar architecture, is closely related to the interfacial materials, because the charge accumulation at interfaces and its capacitive were reported as one of the origins of this effect.[14-16]

TiO_2 is the most widely-used ETM and HBM, and its mesoporous framework is usually employed in the state-of-the-art PSCs.[5,10,17] It generally requires a relatively high temperature sintering process (> 450 °C), which will severely increase the fabrication cost and be unfavourable for the flexible application.[18] Therefore, intensive techniques for the preparation of traditional n-type metal oxides were exploited to realize low-temperature solution deposition.[19-22] Over 15% of PCE was obtained by using TiO_2 particles and ZnO particles as the ETM under 150°C.[19-21] SnO_2 shows even advanced properties, by which exceeding 20% PCE was achieved in a $(FAPbI_3)_{0.97}(MAPbBr_3)_{0.03}$ cell.[22]

Except for metal oxides, alcohol/water soluble conjugated polymers and polyelectrolytes act as the most universal and effective approach for organic solar cells, which are also able to modify the energy level of the contact for PSCs by low-temperature solution deposition.[23] The advantages of these polymeric interfacial materials include good solubility in environmentally friendly solvents, excellent interface modification properties, and the feasibility of the printing technique. PEIE was used to reduce the work function (W.F.) of ITO followed by the deposition of TiO_2 layer as the electron selective layer (ESC), which significantly improved the electronic properties of the device with a remarkable high PCE.[24] Hybrid composite film of the PFN-OX and ZnO was utilized as ESC, and the corresponding PSCs exhibited a PCE of over 16%.[25] However, the above polymeric interfacial materials were not able to perform well without the metal oxide. In addition, despite of their solubility in alcohol/water, themselves suffer from the complexity and difficulty of the synthesize routes, which would cost abundant of organic solvent and thus be environmentally unfriendly during the synthesis process.[23,26]

In this article, a simple polythiophene derivative, sodium poly[2-(3-thienyl)ethyloxy-4-butylsulfonate] (PTEBS), is functioned as the cathode interfacial material for perovskite solar cells individually. (**Figure 1a, 1b**) As expect, favorable energy level alignment and improved interface properties of the modified electron selective contact arises to facilitate the electrons transferring and collecting.[23] Over 15% of PCE was achieved in $CH_3NH_3PbI_3$ based PSCs using PTEBS. Suppressed hysteresis phenomenon is observed due to the reduced charge accumulation at the modified interface. The ionic functionalities give PTEBS advantages such as excellent solubility in water/alcohol (>20 mg/ml) solution and effective ability of interfacial modification via an ultrathin coating. It should also be mentioned that PTEBS can be not only dissolved in water/alcohol but also synthesized in water solvent easily, which meets the economic and

environmental demands for the practical application.[27,28] This work provides a practical candidate of highly-efficient interfacial materials for large-area, low-cost and flexible PSCs, which allows the construction of devices via low-temperature solution process including printing techniques.

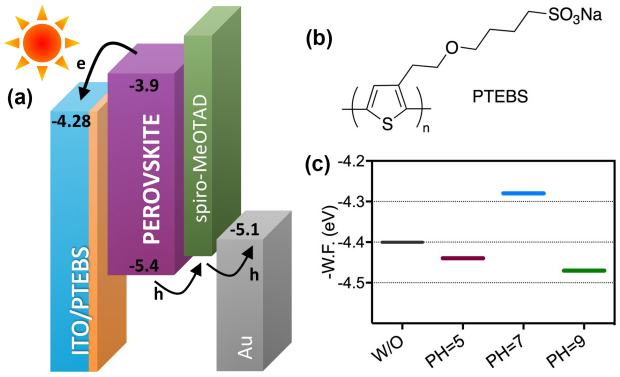

Figure 1. (a) The relative energy level diagram of the perovskite solar cell before and after interface modification with PTEBS; (b) The chemical structure of PTEBS; (c) The work function of PTEBS coated ITO from solutions with various PH.

2. EXPERIMENTAL SECTION

Device Fabrication. Indium doped tin oxide (ITO) glass was cleaned sequentially via detergent, water, acetone, and 2-propanol under ultrasonication for 15 min, and then treated with O_2 plasma for 15 min. 2mg of PTEBS (American Dye Source, Inc.) was dissolved in a 10 mL mixed solution of 2-propanol and ultrapure water (1:2). The PH value was controlled by adding appropriate amount of NaOH or HCl. The interfacial material was deposited on the ITO glass by spin-coating the solution at 4,000 r.p.m. for 30 s, then the film was dried at 110 ºC for 20 min.

The perovskite layer was fabricated by sequential deposition in the atmosphere (humidity<40%). The precursor film was deposited by spin-coating of 1M PbI_2 (99.999%, Alfa Aesar) in DMF at 6000 r.p.m. that was kept at 70 ºC. After drying at 70 ºC, the films were dipped

into a 10mg/mL solution of CH_3NH_3I in 2-propanol (99%, Fisher) kept at 50 ºC for tens of seconds, then dried at 90 ºC for 30 min.

A solution of 2,2',7,7'-tetrakis(*N*,*N*-di-*p*-methoxyphenylamine)-9,9'-spirobifluorene (spiro-MeOTAD)/chlorobenzene (72.3 mg/mL) with 28.8 μL 4-*tert*-butylpyridine, and 17.5 μL Li-TFSI/ acetonitrile (520 mg/mL) was spin-coated at 3500 r.p.m. for 60 s as the standard HTM. Finally, 80 nm Au was thermally evaporated under vacuum to act as the cathode. The active area of the device is determined by a mask of 0.0314 cm^2.

For planar devices with the structure of FTO/TiO_2/Perovskite/spiro-MeOTAD/Au, the clean steps of FTO, perovskite film forming method, deposition of spiro-MeOTAD and Au are the same as the ITO mentioned above. A compact TiO_2 layer was prepared by spin-coating at 4,000 r.p.m. for 30 s using 0.15 M of titanium diisopropoxide bis(acetylacetonate) (75 wt. % in isopropanol, Aldrich) in 1-butanol, dried at 125 ºC for 5 min, then repeated with 0.3 M of titanium diisopropoxide bis(acetylacetonate) solution, finally baked at 500 ºC for 15 min. Then, the resultant TiO_2 film was immersed into a 40 mM $TiCl_4$ aqueous solution at 70 ºC for 30 min, washed with deionized water and ethanol, then baked at 500 ºC for 15 min.

Measurements. *I-V* curves were measured by using Keithley 2611 source meter under simulated sunlight from Oriel 300 solar simulator. The photovoltaic parameters were all obtained by reverse scanning direction from 1.2 V to -0.1 V at the rate of 0.1 V s^{-1} under 100 mW cm^{-2} simulated AM1.5G irradiation if there is no specific illustration. IPCE was measured by using a lock-in amplifier coupled with a monochromator and 500 W xenon lamp (Crowntech, Qtest Station 2000). Both the systems were calibrated against a certified reference solar cell. All the measurements of the solar cells were performed under ambient atmosphere (20%-40% humidity) at room temperature (20-25ºC) without encapsulation. The absorption spectrum was recorded

with UV–visible spectrophotometer (Agilent 8453). The morphology was measured using scanning electron microscope (SEM) (HITACHI 4300). The energy levels were determined by ultraviolet photoelectron spectroscopy (UPS). Electrochemical impedance with the range of 0.1 Hz-1 MHz was performed by PGSTAT302N (Autolab Corp., Switzerland) at the bias of the respective open-circuit voltage under 1 sun illumination. The model and fitting data was obtained by Z-View Analyst software.

3. RESULTS AND DISCUSSIONS

To investigate the role of PTEBS, an ultra-thin coating was deposited on ITO by spin coating from the aqueous/alcohol solution. The W.F. of PTEBS coated ITO films were measured by ultraviolet photoelectron spectroscopy. Since the conformation of the ionic polymer and its energy level can be adjusted by the PH of the solvent, three PH of solutions were adopted to test their different impacts on the W.F.[29] As shown in **Figure 1c**, there is an obvious shift of the W.F. after the deposition of PTEBS. By coating ITO with PTEBS from the acid aqueous solution (PH=5) and alkaline aqueous solution (PH=9), the W.F. downshifts to 4.44 eV and 4.47 eV, respectively. Meanwhile, the ITO/PTEBS film from a neutral aqueous solution (PH=7) exhibits an upshifted W.F. of 4.28 eV. 0.12 eV closer to the vacuum level than that of pristine ITO results in a favourably shrinking energy difference with the LUMO energy level of $CH_3NH_3PbI_3$. It can be deduced that the neutral PTEBS is primarily responsible for the interactions with ITO, which form the interface dipoles resulting in the shift of W.F. When the PTEBS in the ionization environment of acid or alkali, the changes of electronic properties and molecule confirmation and aggregation might cause the inversion of the direction of the interface dipole.[29-31] The energy difference would affect the electron transfer from absorber layer to the cathode and the charge

accumulation at the interface, so that the performance of the solar cells can be manipulated dramatically, which will be discussed in the following.

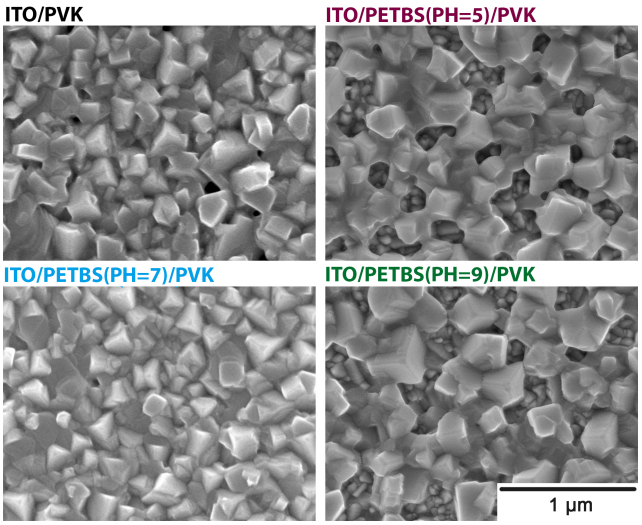

Figure 2. Top-view SEM images of the perovskite (PVK) crystals on substrates with different interfacial materials.

A 250nm-thick $CH_3NH_3PbI_3$ layer was deposited on the PTEBS coated ITO substrates by sequential deposition according to the reported procedure.[32] The scanning electron microscope (SEM) images were used to observe the morphology of the perovskite crystals. As shown in **Figure 2**, perovskite crystals on ITO and ITO/PTEBS(PH=7) exhibit uniform grain size of round 200 nm simultaneously, while distributed pinholes cannot be neglected in the perovskite film on bare ITO substrate. Slightly larger $CH_3NH_3PbI_3$ crystals on the ITO/PTEBS substrates from the acid and alkaline solutions were observed with the grain size of 300 nm and 350 nm, respectively. Much looser arrangement of them indicates the dropped affinity of the substrates. It is obvious that a large area of the substrate is exposed in these two samples, which will cause server

recombination of the holes in the hole transporting layer and the electrons in the contact. Interestingly, the perovskite crystals formed a fully-covered dense film on the ITO/PTEBS(PH=7) in the absence of pinholes (**SI Figure S1**). The crystals are merged compactly in the bottom with a highly-textured surface, on account of which, the photons can be utilized more effectively and the energy loss would be suppressed to a great degree.[20,32]

The UV-vis absorption spectra of the perovskite/interface material/ITO films are displayed in **Figure S2**. Since tiny amounts of the interfacial materials are deposited, the absorbance of them are all below 0.05 in the visible region and negligible to the absorption of the perovskite. Distinct absorptions are detected for the target films in the region of 500 nm-800 nm, and stronger absorptions were found for the films with PTEBS. It can be attributed to the larger perovskite crystals on PTEBS(PH=5,9) and full-covered perovskite on PTEBS(PH=7). Almost equivalent absorbance at 380 nm of the films implied the same amount of PbI_2 precursor on the different substrates, indicating that the morphology difference may occur during the reaction process in the sequential deposition. In the sequential deposition process, the nucleation and crystal growth occurred immediately when the PbI_2 film contacted with the MAI solution. Different ionic properties of the PTEBS surface from different PH solution would affect the interionic distance on the surface, corresponding to distinct nucleation density and surface affinity. Moreover, when the perovskite crystals are growing, the excess ions in the PTEBS(PH=5) and PTEBS(PH=9) might be partially freeing into the solvent adjacent to the subtract as a kind of ionic impurity. Consequently, the crystal growth rate has also been adjusted. As a result, rapid crystal growth rate and decreasing affinity of the substrate are responsible for the reduced coverage in the acid and alkali cases causing by the enlargement of crystals accompanying with the agglomeration. [33]

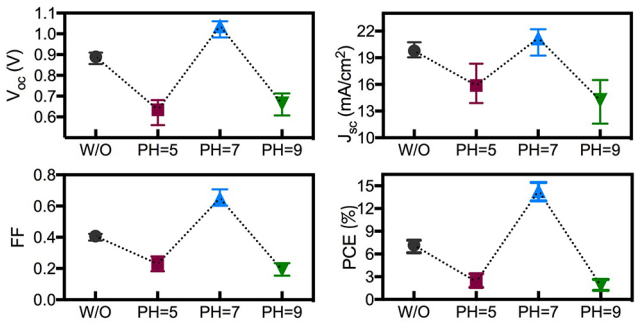

Figure 3. The photovoltaic parameters of the perovskite solar cells based on different interface materials. Each data point represents the average of a set of at least 10 individual devices.

Then, planar perovskite solar cells based on the structure of ITO/PTEBS/$CH_3NH_3PbI_3$/spiro-MeOTAD/Au were fabricated. As a comparison, simplified devices without the interfacial material were also studied. The average performances under 100 mW cm^{-2} simulated AM1.5G irradiation are shown in **Figure 3** and listed in **Table 1**. The average PCE of the simplified W/O device is 7.16%, with an average short-circuit current (J_{sc}) of 19.78 mA cm^{-2}**,** an average fill factor (*FF*) of 0.407, and an average open circuit voltage (V_{oc}) of 0.889 V. By using PTEBS(PH=5) and PTEBS(PH=9) to modify the interface, even worse performance was observed with a low average PCE of 2.35% and 1.83%, respectively. Interestingly, significant improvements are achieved in the device containing PTEBS(PH=7) with a relatively high average PCE of 14.3%, J_{sc} of 21.23 mA cm^{-2}, V_{oc} of 1.038 V, and *FF* of 0.651. Note that the parameters of these devices exhibit highly consistent with the W.F. of the ESCs (**Figure 3**), demonstrating the validity of the energy level engineering for increasing the device performance of PSCs.

Table 1. The average and the best photovoltaic performances of the devices. The averages came from a set of at least 10 individual devices.

Device		V_{oc} (V)	J_{sc} (mA cm^{-2})	FF	PCE (%)	R_s (Ω•cm^2)	R_{sh} (Ω•cm^2)
W/O	average	0.889±0.021	19.78±0.45	0.407±0.016	7.16±0.46	22.1±2.3	372±69
	best	0.893	20.74	0.422	7.81	19.8	333
PTEBS(PH=5)	average	0.634±0.039	15.89±1.42	0.230±0.030	2.35±0.58	48.2±12.3	51.9±13.1
	best	0.671	18.33	0.277	3.40	33.1	76.1
PTEBS(PH=7)	average	1.038±0.020	21.23±0.63	0.651±0.029	14.3±0.60	6.18±0.95	675±24
	best	1.026	21.79	0.690	15.4	5.95	700
PTEBS(PH=9)	average	0.663±0.035	14.20±1.56	0.191±0.029	1.83±0.49	52.7±10.2	39.6±8.4
	best	0.713	16.50	0.226	2.66	37.9	43.0

Highly efficient perovskite solar cells require the perovskite film composed of highly-qualitied large crystallites as well as with a full coverage on the substrate. Neither can be dispensable.[5-7,32] The former guarantees efficient light absorption and fast carrier transfer in the perovskite film; The latter prevented the recombination of the holes in spiro-MeOTAD and the electrons in ITO/PTEBS film. In the PTEBS(PH=5) and PTEBS(PH=9) cases, the bareness of the substrate between loosen arranged crystallites causes serious charge recombination and energy loss in the devices. It is well known that V_{oc} is determined by the quasi-Fermi level difference between the hole selective layer and the electron selective layer. The introduction of PTEBS(PH=7) reduces the W.F. of the ESC. Thus, the average V_{oc} of PETBS(PH=7) devices reaches 1.038 V, which is quite high for $CH_3NH_3PbI_3$ based devices. The optimal perovskite morphology minimizing the charge recombination in devices should be another important factor to reach such high V_{oc}. The modified ESC also formed a better ohmic contact at the interface in

the light of decreased serious resistance (R_s) and increased shunt resistance (R_{sh}) (**Table 1**).[25] The best performed PETBS device reaches a PCE of 15.4%, a J_{sc} of 21.79 mA cm^{-2}, V_{oc} of 1.026 V, and *FF* of 0.690.

It's believed that PTEBS performs as the interfacial modifier, instead of the electron transporting material. Firstly, the work function of the ITO/PTEBS substrate is quite different with the LUMO energy level of PTEBS itself,[34] because the thickness of the PTEBS coating should be below 2 nm in our cases.[29] Therefore, the coating of PTEBS on the ITO cannot form a complete layer of film with such thin thickness. Secondly, PTEBS is used to be the electronic donor in the reported organic solar cells and almost an insulating polymer.[35] Devices with a slightly thicker PTEBS displayed a precipitous decline of *FF* (**Figure S3**), representing a dramatic increase of the serious resistance.

Moreover, the devices employing PTEBS also show excellent stability and reproducibility. (**SI Figure S4, S5**) Further enhancement for the performance of the PTEBS based device should be built on the optimal composition of the perovskite.

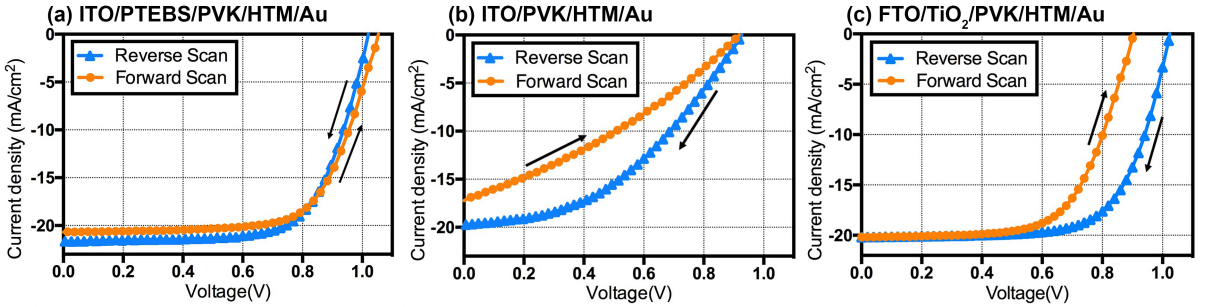

Scan	V_{oc} (V)	J_{sc} (mA cm^{-2})	*FF*	PCE (%)
Reverse	1.021	21.64	0.679	15.0
Forward	1.054	20.67	0.678	14.8

Scan	V_{oc} (V)	J_{sc} (mA cm^{-2})	*FF*	PCE (%)
Reverse	0.910	19.50	0.421	7.51
Forward	0.920	17.21	0.321	5.07

Scan	V_{oc} (V)	J_{sc} (mA cm^{-2})	*FF*	PCE (%)
Reverse	1.024	20.18	0.682	14.1
Forward	0.904	20.17	0.639	11.7

Figure 4. *I–V* curves and performances of perovskite (PVK) solar cells by reverse and forward scanning directions at the rate of 0.1 V s^{-1}.

As to a planar PSC, the hysteresis is an important concern. Hence, we investigated the performance difference of the devices by reverse and forward scanning directions (**Figure 4**). As a comparison, device with the most common election selective layer of TiO_2 was also fabricated. We tested the PTEBS(PH=7) device with a representative PCE of 15.0% by reverse scan, of which the *I-V* curve is almost coincided with that by forward scan with a PCE of 14.8%. However, both the simplified W/O devices and TiO_2 device show pronounced hysteresis phenomenon as seen in **Figure 4b**, caused by the huge mismatches on *FF* and V_{oc}, respectively. The different hysteresis behavior demonstrates that the interfacial material plays a vital role on the hysteresis effect. The hysteresis behavior is also reflected in the incident photon-to-current efficiency (IPCE) spectrum (**SI Figure S6**). For the PTEBS(PH=7) device, the current density of 20.33 mA cm^{-2} calculated from the IPCE is in good agreement with 20.67 mA cm^{-2} by *I–V* curve. At the same time, an extremely large mismatch of 2.20 mA cm^{-2} of current density is found for the W/O device.

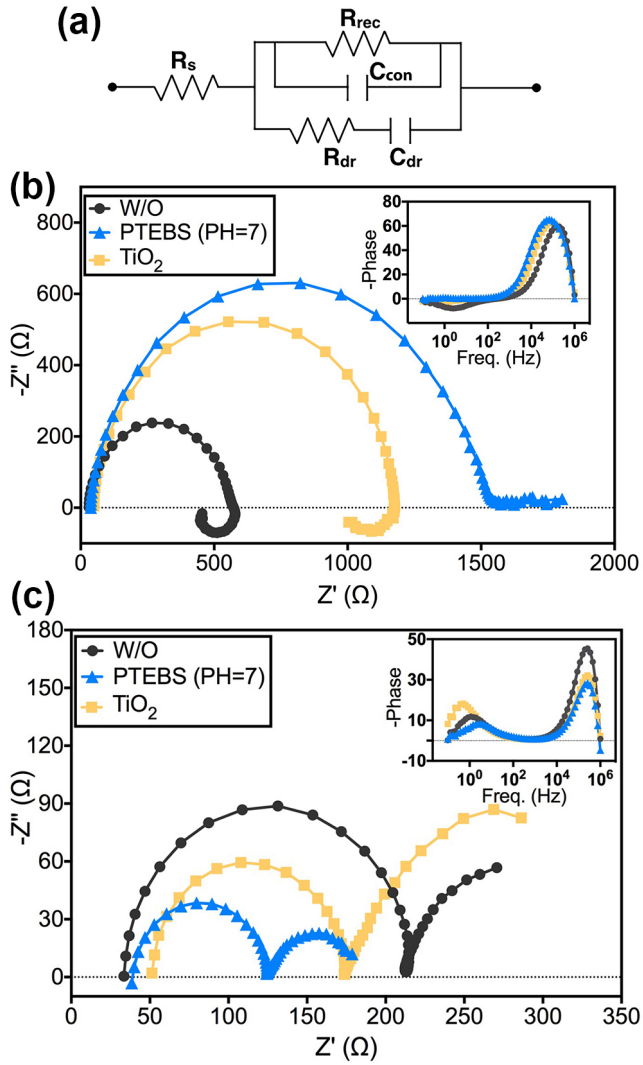

Figure 5. (a) The equivalence circuit for fitting the impedance response using the Debye relaxation model. Nyquist plots and bode plots (the insertion) of perovskite solar cells with different interface materials measuring (b) in the dark and (c) under 1 sun illumination at the respective V_{oc}.

To further study the functions of PTEBS, the electrochemical impedance spectrum (EIS) was performed to reflect the charge transport and accumulation process and how it suppresses the anomalous hysteresis behavior. According to the Debye relaxation model, the high-frequency region is mainly suggested to the interface charge between the perovskite and the charge-

selective contact; the low-frequency region, which represents a slow dynamic, is the response from the dielectric polarization of the perovskite material or the ion immigration.[15] We used the equivalent-circuit to describe these features, including the series resistance (R_s), the interfacial recombination resistance (R_{rec}), the selective contact capacitance (C_{con}), the dielectric relaxation resistance (R_{dr}) and the dielectric contact capacitance (C_{dr}) (**Figure 5a**).[16]

Table 2. The values of fitted parameters from the EIS.

Condition	Device	R_s ($\Omega \cdot cm^2$)	R_{rec} ($\Omega \cdot cm^2$)	C_{con} ($F \cdot cm^{-2}$)	R_{dr} ($\Omega \cdot cm^2$)	C_{dr} ($F \cdot cm^{-2}$)
Dark	W/O	34.3	561	8.85×10^{-9}	-	-
	PTEBS(PH=7)	40.5	1.52×10^{3}	1.05×10^{-8}	-	-
	TiO_2	51.8	1.18×10^{3}	9.39×10^{-9}	-	-
Illumination	W/O	36.4	287	1.03×10^{-8}	464	1.68×10^{-4}
	PTEBS(PH=7)	42.8	130	1.61×10^{-8}	222	1.38×10^{-4}
	TiO_2	53.6	280	1.06×10^{-8}	217	5.83×10^{-4}

The measurement was firstly taken in the dark at the respective V_{oc}. The arc was found in the high-mid frequency relating to the charge transport at the perovskite/ESC interface (**Figure 5b**). A large R_{rec} represents that the charge recombination can be restrained more effectively for PTEBS(PH=7) device (**Table 2**).[36] Distinct features in the low frequency area representing negative capacitance are observed for W/O and TiO_2 device, whose origin is still under debate.[16,37] But in our case, we believe the more serious inductive behavior in the EIS may correspond to the more pronounced hysteresis phenomenon. Two arcs were found in the spectrums under 1 sun illumination (**Figure 5c**). R_{dr} and C_{dr} regarding the slow dielectric relaxation in the low-frequency region are proposed to associate with the hysteresis behavior, and can be used to describe the electric polarization in the perovskite adjacent to the ESC. **Table 2** shows the values of fitted parameters. Lower values of R_{dr} and C_{dr} for PTEBS (PH=7) device than those of the W/O device intimated the weaker polarization of the perovskite, and the polarization can be released more easily. The R_{dr} values of PTEBS (PH=7) device and the TiO_2

device are very close, but the value C_{dr} of the latter device is much larger than the former, which reveals the intensive charge accumulating at the perovskite/TiO_2 interface. Accordingly, we assumed that PTEBS likely impairs the charge accumulation and relating electric field at the perovskite/ESC interface. Thus, weaker electric polarization contributes to the hysteresis resulting in a quicker response of PTEBS devices. [15,16]

4. CONCLUSIONS

In summary, a water-soluble polythiophene, PTEBS, was developed as a novel cathode interfacial material for planar perovskite solar cells. Owing to the modified n-type contact, better energy level alignment and optimized morphology of perovskite crystals contribute to the significant performance improvement for $CH_3NH_3PbI_3$ based cells with the highest PCE exceeding 15%. Besides, the anomalous hysteresis effect can be eliminated to a large degree due to less charge accumulation at interface. This work provides a valid interfacial material for the construction of large-area, low-cost and flexible PSCs, which allows for low-temperature solution methods and roll-to-roll manufacture.

ASSOCIATED CONTENT

Supporting Information

The following files are available free of charge.

cross-sectional SEM image, UV-vis absorption spectra, device stability, device reproducibility, IPCE spectrums, the performance of devices.

AUTHOR INFORMATION

Corresponding Author

*(L. Xiao) Email: xiao66@pku.edu.cn

*(Y. Wang) Email: yuanhaowang@yahoo.com

Author Contributions

The manuscript was written through contributions of all authors. All authors have given approval to the final version of the manuscript.

Funding Sources

Natural Science Foundation of China (61605164 and 61575005)

Shenzhen Peacock Plan (KQTD2015071616442225)

ACKNOWLEDGMENT

We acknowledge the financial support from the Natural Science Foundation of China (61605164 and 61575005), the Postdoctoral Science Foundation of China, the Hong Kong Scholar Programme, and Shenzhen Peacock Plan (KQTD2015071616442225)

REFERENCES

(1) Stranks, S. D.; Eperon, G. E.; Grancini, G.; Menelaou, C.; Alcocer, M. J. P.; Leijtens, T.; Herz, L. M.; Petrozza, A.; Snaith, H. J. Electron-Hole Diffusion Lengths Exceeding 1 Micrometer in an Organometal Trihalide Perovskite Absorber. *Science* **2013**, *342*, 341–344.

(2) Xing, G.; Mathews, N.; Sun, S.; Lim, S. S.; Lam, Y. M.; Gräztel, M.; Mhaisalkar, S.; Sum, T. C. Long-Range Balanced Electron- and Hole-Transport Lengths in Organic-Inorganic $CH_3NH_3PbI_3$. *Science* **2013**, *342*, 344–347.

(3) Baikie, T.; Fang, Y.; Kadro, J. M.; Schreyer, M.; Wei, F.; Mhaisalkar, S. G.; Gräztel, M.; White, T. J. Synthesis and Crystal Chemistry of the Hybrid Perovskite $(CH_3NH_3)PbI_3$ for Solid-State Sensitised Solar Cell Applications. *J. Mater. Chem. A* **2013**, *1*, 5628-5641.

(4) NREL. Best Research-Cell Efficiencies http://www.nrel.gov/ncpv/images/efficiency_chart.jpg (accessed Feb 01, 2017).

(5) Li, X.; Bi, D.; Yi, C.; Décoppet, J.-D.; Luo, J.; Zakeeruddin, S. M.; Hagfeldt, A.; Gräztel, M. A Vacuum Flash-Assisted Solution Process for High-Efficiency Large-Area Perovskite Solar Cells. *Science* **2016**, *353*, 58-62.

(6) Bi, D.; Yi, C.; Luo, J.; Décoppet, J.-D.; Zhang, F.; Zakeeruddin, S. M.; Li, X.; Hagfeldt, A.; Gräztel, M. Polymer-Templated Nucleation and Crystal Growth of Perovskite Films for Solar Cells with Efficiency Greater than 21%. *Nat. Energy* **2016**, *1*, 16142.

(7) Zheng, L.; Zhang, D.; Ma, Y.; Lu, Z.; Chen, Z.; Wang, S.; Xiao, L.; Gong, Q. Morphology Control of the Perovskite Films for Efficient Solar Cells. *Dalton Trans.* **2015**, *44*, 10582-10593.

(8) Jeon, N. J.; Lee, H. G.; Kim, Y. C.; Seo, J.; Noh, J. H.; Lee, J.; Seok, S. I. *o*-Methoxy Substituents in spiro-OMeTAD for Efficient Inorganic-Organic Hybrid Perovskite Solar Cells. *J. Am. Chem. Soc.* **2014**, *136*, 7837-7840.

(9) Chueh, C.-C.; Li, C.-Z.; Jen, A. K.-Y. Recent Progress and Perspective in Solution-processed Interfacial Materials for Efficient and Stable Polymer and Organometal Perovskite Solar Cells. *Energy Environ. Sci.* **2015**, *8*, 1160-1189.

(10) Saliba, M.; Matsui, T.; Domanski, K.; Seo, J.-Y.; Ummadisingu, A.; Zakeeruddin, S. M.; Correa-Baena, J.-P.; Tress, W. R.; Abate, A.; Hagfeldt, A.; Gräztel, M. Incorporation of Rubidium Cations into Perovskite Solar Cells Improves Photovoltaic Performance. *Science* **2016**, *354*, 206-209.

(11) Bella, F.; Griffini, G.; Correa-Baena, J.-P.; Saracco, G.; Gräztel, M.; Hagfeldt, A;. Turri, S.; Gerbaldi, C. Improving Efficiency and Stability of Perovskite Solar Cells with Photocurable Fluoropolymers. *Science* **2016**, DOI: 10.1126/science.aah4046.

(12) Pascoe, A. R.; Duffy, N. W.; Scully, A. D.; Huang, F.; Cheng, Y.-B. Insights into Planar $CH_3NH_3PbI_3$ Perovskite Solar Cells Using Impedance Spectroscopy. *J. Phys. Chem. C* **2015**, *119*, 4444-4453.

(13) Ma, Y.; Chung, Y.-H.; Zheng, L.; Zhang, D.; Yu, X.; Xiao, L.; Chen, Z.; Wang, S.; Qu, B.; Gong, Q.; Zou, D. Improved Hole-Transporting Property via HAT-CN for Perovskite Solar Cells without Lithium Salts. *ACS Appl. Mater. Interfaces* **2015**, *7*, 6406–6411.

(14) Yang, G.; Lei, H.; Tao, H.; Zheng, X.; Ma, J.; Liu, Q.; Ke, W.; Chen, Z.; Xiong, L.; Qin, P.; Chen, Z.; Qin, M.; Lu, X.; Yan, Y.; Fang, G. Reducing Hysteresis and Enhancing

Performance of Perovskite Solar Cells Using Low-Temperature Processed Y-Doped SnO_2 Nanosheets as Electron Selective Layers. *Small* **2017**, *13*, 1601769.

(15) Sepalage, G. A.; Meyer, S.; Pascoe, A.; Scully, A. D.; Huang, F.; Bach, U.; Cheng, Y.-B.; Spiccia, L. Copper (I) Iodide as Hole-Conductor in Planar Perovskite Solar Cells: Probing the Origin of J-V Hysteresis. *Adv. Funct. Mater.* **2015**, *25*, 5650-5661.

(16) Bisquert, J.; Bertoluzzi, L.; Mora-Sero, I.; Garcia-Belmonte, G. Theory of Impedance and Capacitance Spectroscopy of Solar Cells with Dielectric Relaxation, Drift-Diffusion Transport, and Recombination. *J. Phys. Chem. C* **2014**, *118*, 18983-18991.

(17) Yi, C.; Li, X.; Luo, J.; Zakeeruddin, S. M.; Gräztel, M. Perovskite Photovoltaics with Outstanding Performance Produced by Chemical Conversion of Bilayer Mesostructured Lead Halide/TiO_2 Films. *Adv. Mater.* **2016**, *28*, 2964-2970.

(18) Xu, X.; Chen, Q.; Hong, Z.; Zhou, H.; Liu, Z.; Chang, W.-H.; Sun, P.; Chen, H.; Marco, N. D.; Wang, M.; Yang, Y. Working Mechanism for Flexible Perovskite Solar Cells with Simplified Architecture. *Nano Lett.* **2015**, *15*, 6514-6520.

(19) Wojciechowski, K.; Saliba, M.; Leijtens, T.; Abate, A.; Snaith, H. J. Sub-150 °C Processed Meso-Superstructured Perovskite Solar Cells with Enhanced Efficiency. *Energy Environ. Sci.* **2014**, *7*, 1142-1147.

(20) Liu, D.; Kelly, T. L. Perovskite Solar Cells with a Planar Heterojunction Structure Prepared Using Room-Temperature Solution Processing Techniques. *Nat. Photonics* **2014**, *8*, 133-138.

(21) Yang, D.; Yang, R.; Zhang, J.; Yang, Z.; Liu, S.; Li, C. High Efficiency Flexible Perovskite Solar Cells Using Superior Low Temperature TiO_2. *Energy Environ. Sci.* **2015**, *8*, 3208-3214.

(22) Jiang, Q.; Zhang, L.; Wang, H.; Yang, X.; Meng, J.; Liu, H.; Yin, Z.; Wu, J.; Zhang, X.; You, J. Enhanced Electron Extraction Using SnO_2 for High-Efficiency Planar-Structure $HC(NH_2)_2PbI_3$-Based Perovskite Solar Cells. *Nat. Energy* **2016**, *2*, 16177.

(23) Duan, C.; Zhang, K.; Zhong, C.; Huang, F.; Cao, Y. Recent Advances in Water/alcohol-Soluble π-Conjugated Materials: New Materials and Growing Applications in Solar Cells. *Chem. Soc. Rev.* **2013**, *42*, 9071-9104.

(24) Zhou, H.; Chen, Q.; Li, G.; Luo, S.; Song, T.; Duan, H.-S.; Hong, Z.; You, J.; Liu, Y.; Yang, Y. Interface Engineering of Highly Efficient Perovskite Solar Cells. *Science* **2014**, *345*, 542-546.

(25) Hu, Q.; Liu, Y.; Li, Y.; Ying, L.; Liu, T.; Huang, F.; Wang, S.; Huang, W.; Zhu, R.; Gong, Q. Efficient and Low-Temperature Processed Perovskite Solar Cells Based on a Cross-Linkable Hybrid Interlayer. *J. Mater. Chem. A* **2015**, *3*, 18483-18491.

(26) Huang, F.; Wu, H.; Wang, D.; Yang, W.; Cao, Y. Novel Electroluminescent Conjugated Polyelectrolytes Based on Polyfluorene. *Chem. Mater.* **2004**, *16*, 708-716.

(27) Tran-Van, F.; Carrier, M.; Chevrot, C. Sulfonated Polythiophene and Poly(3,4-ethylenedioxythiophene) Derivatives with Cations Exchange Properties. *Synth. Met.* **2004**, *142*, 251-258.

(28) Zhao, Y.; Zhu, H.; Wang, X.; Liu, Y.; Wu, X.; Zhou, H.; Ni, Z. Enzyme-Catalyzed Synthesis of Water-Soluble Conjugated Poly[2-(3-thienyl)-Ethoxy-4-Butylsulfonate]. *Polymers* **2016**, *8*, 139.

(29) Kozlovskaya, V.; Kharlampieva, E.; Jones, K.; Lin, Z.; Tsukruk, V. V. pH-Controlled Assembly and Properties of LbL Membranes from Branched Conjugated Poly(alkoxythiophene sulfonate) and Various Polycations. *Langmuir* **2010**, *26*, 7138-7147.

(30) Zhou, Y.; Fuentes-Hernandez, C.; Shim, J.; Meyer, J.; Giordano, A. J.; Li, H.; Winget, P.; Papadopoulos, T.; Cheun, H.; Kim, J.; Fenoll, M.; Dindar, A.; Haske, W.; Najafabadi, E.; Khah, T. M.; Sojoudi, H.; Barlow, S.; Graham, S.; Brédas, J.-L.; Marder, S. R.; Kahn, A.; Kippelen, B. A Universal Method to Produce Low–Work Function Electrodes for Organic Electronics. *Science* **2012**, *336*, 327-332.

(31) Schwartz, B. J. Conjugated Polymers as Molecular Materials: How Chain Conformation and Film Morphology Influence Energy Transfer and Interchain Interactions. *Annu. Rev. Phys. Chem.* **2003**, *54*, 141– 172.

(32) Zheng, L.; Ma, Y.; Chu, S.; Wang, S.; Qu, B.; Xiao, L.; Chen, Z.; Gong, Q.; Wu, Z.; Hou, X. Improved Light Absorption and Charge Transport for Perovskite Solar Cells with Rough Interfaces by Sequential Deposition. *Nanoscale* **2014**, *6*, 8171-8176.

(33) Abbona, F.; Aquilano, D.; In *Springer Handbook of Crystal Growth*; Dhanaraj, G., Byrappa, K., Prasad, V., Dudley, M., Eds.; Springer: Berlin, 2010 ; Chapter 3, pp 53-86.

(34) Qiao, Q. and McLeskey, T. Water-soluble Polythiophene/nanocrystalline TiO_2 Solar Cells. *Appl. Phys. Lett.* **2005**, *86*, 153501.

(35) Chayer, M.; Faïd K.; Leclerc, M. Highly Conducting Water-Soluble Polythiophene Derivatives. *Chem. Mater.* **1997**, *9*, 2902-2905.

(36) Yang, D.; Zhou, X.; Yang, R.; Yang, Z.; Yu, W.; Wang, X.; Li, C.; Liu, S.; Chang, R. P. H. Surface Optimization to Eliminate Hysteresis for Record Efficiency Planar Perovskite Solar Cells. *Energy Environ. Sci.* **2016**, *9*, 3071-3078.

(37) Sanchez, R. S.; Gonzalez-Pedro, V.; Lee, J.-W.; Park, N.-G.; Kang, Y. S.; Mora-Sero, I.; Bisquert, J. Slow Dynamic Processes in Lead Halide Perovskite Solar Cells. Characteristic Times and Hysteresis. *J. Phys. Chem. Lett.* **2014**, *5*, 2357-2363.

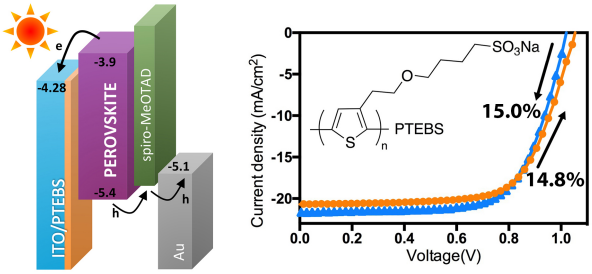

A water soluble polythiophene, PTEBS was employed as an efficient interfacial material for planar perovskite solar cells by an all low-temperature process without apparent hysteresis effect.